Available online at www.sciencedirect.com
ScienceDirect
Medical Engineering & Physics 30 (2008) 350–357
Medical Engineering & Physics
www.elsevier.com/locate/medengphy

A novel automatic image processing algorithm for detection of hard exudates based on retinal image analysis

Clara I. Sánchez [a,*], Roberto Hornero [a], María I. López [b], Mateo Aboy [c], Jesús Poza [a], Daniel Abásolo [a]

[a] *Grupo de Ingeniería Biomédica, E.T.S. Ingenieros de Telecomunicación, Universidad de Valladolid, Spain*
[b] *Instituto de Oftalmobiología Aplicada (IOBA), Universidad de Valladolid, Spain*
[c] *Department of Electrical Engineering at Oregon Institute of Technology, Portland, OR, USA*

Received 30 October 2006; received in revised form 26 March 2007; accepted 7 April 2007

Abstract

We present an automatic image processing algorithm to detect hard exudates. Automatic detection of hard exudates from retinal images is an important problem since hard exudates are associated with diabetic retinopathy and have been found to be one of the most prevalent earliest signs of retinopathy. The algorithm is based on Fisher's linear discriminant analysis and makes use of colour information to perform the classification of retinal exudates. We prospectively assessed the algorithm performance using a database containing 58 retinal images with variable colour, brightness, and quality. Our proposed algorithm obtained a sensitivity of 88% with a mean number of 4.83 ± 4.64 false positives per image using the lesion-based performance evaluation criterion, and achieved an image-based classification accuracy of 100% (sensitivity of 100% and specificity of 100%).

Keywords: Diabetic retinopathy; Hard exudates; Image processing; Retinal images

1. Introduction

Diabetic retinopathy (DR) is the most common cause of blindness and vision defects in developed countries [1]. Due to its prevalence and clinical significance the research community has attempted to improve its diagnosis and treatment by developing algorithms to perform retinal image analysis, fundus image enhancement [2–4], and monitoring [5]. Of special significance are automatic image analysis algorithms designed to detect hard exudates (HEs) [6]. HEs have been found to be the most specific markers for the presence of retinal oedema, the major cause of visual loss in non-proliferative forms of DR [1]. Additionally, HEs are one of the most prevalent lesions during early stages of DR [1].

Automatic algorithms for HE detection are required in a variety of applications including the design of complete systems for automatic processing of retinal images. Several techniques have been developed for HE detection in fundus images based on a variety of techniques [6]. These techniques include the usage of image contrast and brightness analysis [7–13], Bayesian classifiers [14,15], and neural networks [16,17].

In this paper, we propose a novel automatic image processing algorithm for detection of HEs based on retinal image analysis. The algorithm employs statistical recognition and colour information to detect retinal exudates. Our proposed algorithm does not require user initialization and is robust to the changes in the appearance of retinal fundus images typically encountered in clinical environments.

In Section 2, we describe the exudates detection algorithm in detail. Sections 3 and 4 report the performance results, and Section 5 discusses the contributions and limitations of the algorithm.

* Corresponding author at: E.T.S. Ingenieros de Telecomunicación, Universidad de Valladolid, Camino del Cementerio s/n, 47011 Valladolid, Spain.
E-mail address: csangut@gmail.com (C.I. Sánchez).

1350-4533/$ – see front matter © 2007 IPEM. Published by Elsevier Ltd. All rights reserved.
doi:10.1016/j.medengphy.2007.04.010

2. Hard exudates detection

Our proposed algorithm for HEs detection is composed of four main stages: (1) image preprocessing and enhancement, (2) feature extraction, (3) classification, and (4) postprocessing. In the first stage, the image is enhanced to obtain adequate illumination normalization and contrast. Following this step, the algorithm extracts dynamical training sets from each image. Next, the algorithm classifies the pixels using a Fisher's linear discriminant. Finally, a postprocessing technique is applied to distinguish HEs from cotton wool spots (CWs) and other artefacts.

2.1. Preprocessing stage

The preprocessing stage is crucial to the algorithm success due to the intrinsic characteristics of the retinal images. For instance, due to the strong correlation between skin pigmentation and iris colour, the colour of fundus from different subjects is typically unique.

Additionally, retinal images are often poorly contrasted. The contrast of fundus images diminishes as distance of a pixel from the centre of the image increases. The uneven illumination raises the intensity levels in the regions near the optic disk (OD) but gradually reduces the brightness when distance to the OD is increased. All these features have a significant impact on the detection of retinal lesions, especially HEs.

Colour normalization and contrast enhancement of the fundus photographs are needed before starting exudate detection. Instead of applying grey-scale techniques independently to each colour component, our algorithm uses a modification of the RGB model to obtain colour normalization and contrast enhancement resulting in a set of new $(R_{mod}, G_{mod}, B_{mod})$ component as follows:

$$\begin{aligned} &(R,\ G,\ B) \rightarrow (Y,\ I,\ Q)\\ &Y_{mod} = aY + bI + cQ\\ &(Y_{mod},\ I,\ Q) \rightarrow (R_{mod},\ G_{mod},\ B_{mod}). \end{aligned} \tag{1}$$

where (R, G, B) are the three components of the original RGB model, (Y, I, Q) the components of the YIQ model and $\rightarrow$ defines the conversion of one colour space into another [18]. This transformation avoids the problems associated with applying grey-scale methods to each of the components due to the high correlation between components [19]. In this transformation a, b and c are parameters which depend on the characteristics of the images. They are selected to reduce the local luminance variability (σ_μ) throughout Y_{mod} and increase the mean contrast levels (μ_σ and μ_c) within it [4]. Applying the parameters $[a, b, c] = [1.5, -1, -1]$, the standard deviation of the local luminosity σ_μ in Y_{mod} decreases 6.10% compared to the original luminance component whereas the contrast levels μ_σ and μ_c increase 25.17% and 24.55%, respectively. The resulting image (Fig. 1(a and b)) shows an improvement in the overall colour saturation and in the contrast between lesions and background.

2.2. Feature selection and extraction

As HEs are mainly characterized by their colour, we used colour features to define the feature space. The selection of these features is a complicated task due to the variety of colour models. In order to select one of these models objectively we calculated a quantitative metric (J) to evaluate the performance of different colour spaces. The metric J estimates the class separability of exudate and non-exudate pixels in different colour spaces using within-class and between-class scatter matrices [20], as follows:

$$J = \mathrm{trace}\left(\frac{S_\mathrm{b}}{S_\mathrm{w}}\right) \tag{2}$$

where S_b and S_w are the between-class and within-class scatter matrices, respectively. A higher value of J indicates that the classes are more separated while members within each class are closer to each other. Applying this metric to several colour models, we have obtained the highest value for the new model $\mathrm{R_{mod}G_{mod}B_{mod}}$ (Table 1). Therefore, the proposed modification of the RGB model is the most suitable colour model for our retinal image analysis. A three-dimensional feature vector $\boldsymbol{X}$ is defined for each pixel made up of its components in the $\mathrm{R_{mod}G_{mod}B_{mod}}$ model.

Two training sets representative of our classification problem have to be selected: a non-exudate and an exudate sets. When the training sets are obtained manually, only a group of images are used to extract them. Due to the large intra-class variability among images, even after the preprocessing stage, these datasets are not representative of the characteristics of all the images. Our proposed algorithm overcomes this problem by automatically extracting several training sets from each image, avoiding manual segmentation.

For each image, the exudate training set is made up by pixels belonging to small isolated exudates. Their characteristics can represent the rest of exudates in the image. Additionally, this type of exudates can be found in all the fundus images with HEs, even in the earliest stages of DR. The exudate training set is obtained carrying out a coarse segmentation of the image. First, exudate edges in the image are enhanced applying Frei–Chen operator [21], which highlights the edges

Table 1
Class separability quantitative metric

Color model	RGB	HSI	YIQ	YCbCr	Lab	Luv	$\mathrm{R_{mod}G_{mod}B_{mod}}$
J	2.91	2.98	2.91	2.92	2.99	2.49	4.14

Quantitative analysis of class separability of exudates and non-exudates pixels using a manually and randomly segmented dataset of 1487 exudates pixels and 1873 non-exudates pixels.

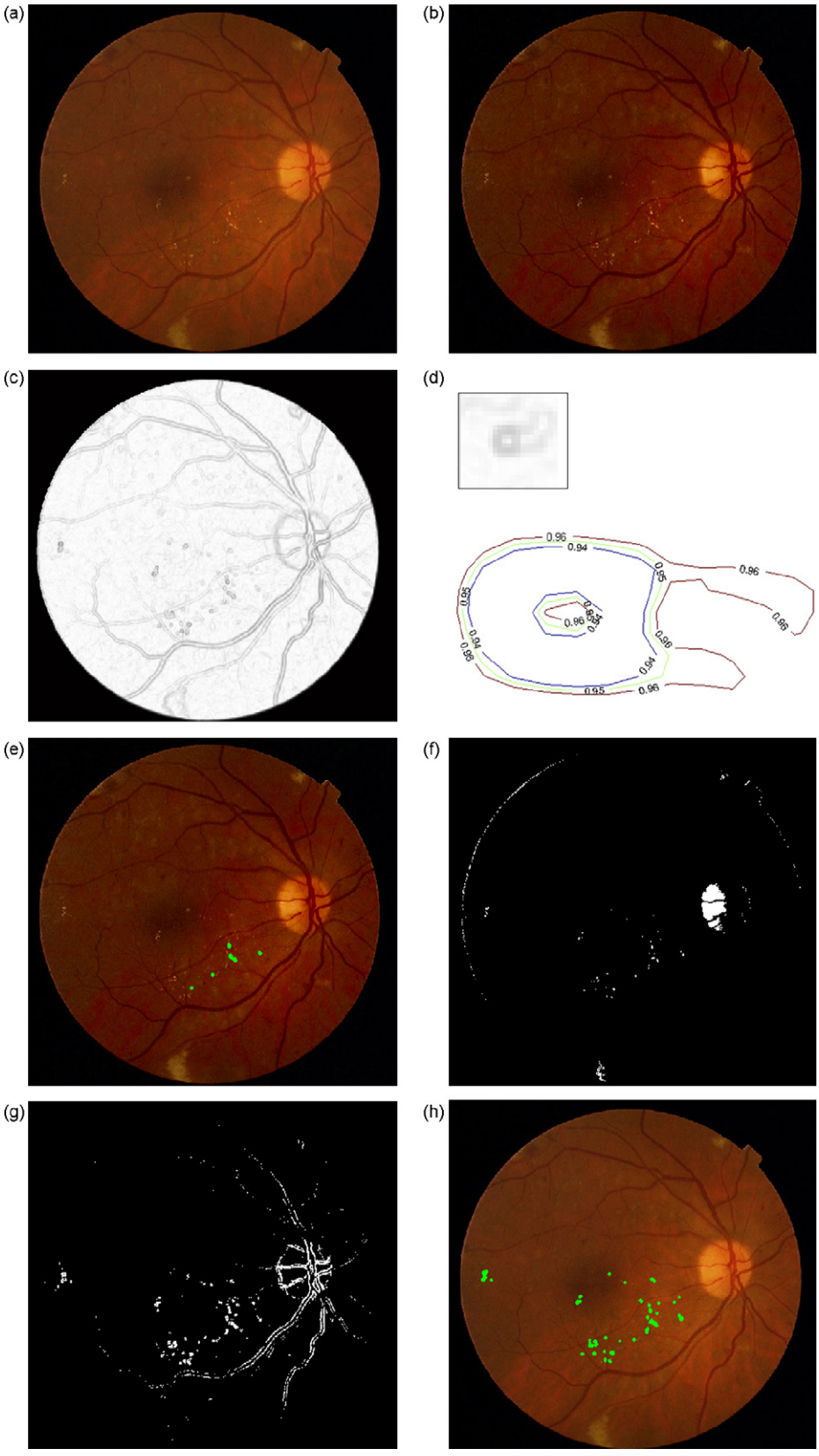

Fig. 1. Detection of hard exudates: (a) original image, (b) image after enhancement, (c) edge enhancement using Frei–Chen operator (I_{frei}), (d) example of an isolated exudate in I_{frei} and its representation as a height map, (e) detected exudates for the training set (in green), (f) result after classification task (I_{class}), (g) detection of objects with sharp edges ($I_{edge\_strength}$) and (h) final result of the exudate detection algorithm. (For interpretation of the references to color in this figure legend, the reader is referred to the web version of the article.)

independently of the brightness magnitude (Fig. 1(c)):

$$I_{\text{frei}}(m,\ n) = \cos^{-1}\left[\frac{\sum_{i=1}^{4}(\boldsymbol{v}_i \cdot \boldsymbol{r}_{mn})^2}{\sum_{i=1}^{9}(\boldsymbol{v}_i \cdot \boldsymbol{r}_{mn})^2}\right]^{1/2} \tag{3}$$

where $\boldsymbol{r}_{mn}$ is a vector which represents a 3×3 subimage of R_{mod} centred in the pixel (m, n), $\boldsymbol{v}_i$ with $i = 1, \ldots, 9$ are the Frei–Chen masks in $\Re^9$ and $\boldsymbol{v}_i$ with $i = 1, \ldots, 4$ form the Frei–Chen edge subspace [21]. The red component of the modified RGB model, R_{mod}, is used because HEs appear with higher intensity and with a more homogenous background. As shown in Fig. 1(d), the exudates are characterized by a white region totally surrounded by a dark grey area, especially small isolated exudates. Treating the result as a height map (Fig. 1(d)), we can detect isolated exudates identifying groups of bright pixels surrounded by iso-height descending closed curves. These pixels $\{\boldsymbol{X}_{\text{ex}}^1, \ldots, \boldsymbol{X}_{\text{ex}}^N\}$, which are shown in Fig. 1(e), form the exudate training set. The size N of this training set varies from image to image depending on the course segmentation and the number of isolated pixels found.

The non-exudates training set $\{\boldsymbol{X}_{\text{non\_ex}}^1, \ldots, \boldsymbol{X}_{\text{non\_ex}}^M\}$ is chosen by selecting M pixels around the OD, where M depends on the OD area. Although these pixels are not strongly representative for the non-exudate class, they are closer to the exudate pixels in the feature space (Fig. 2). Consequently, the decision boundary is placed more accurately between the two classes, obtaining a better performance of the classification task.

2.3. Classification

In this step, the algorithm performs the classification between the two classes (i.e. exudates and non-exudates) using the different training sets extracted from each image.

Since screening of DR is performed on large number of images, it is important that the classification is time efficient. To account for the time constrains the algorithm employs a Fisher's linear discriminant (FLD) due to its time efficiency. In addition to its time efficiency, the FLD takes into account the shape of the clusters in the feature space (Fig. 2). Specifically, the FLD seeks a direction w of the data in the feature space that maximizes the class separability [22]. This direction w is found maximizing the function:

$$J(w) = \frac{w^{\text{T}} S_{\text{b}} w}{w^{\text{T}} S_{\text{w}} w} \tag{4}$$

where S_{b} is the between-class scatter matrix:

$$S_{\text{b}} = (\mu_{\text{ex}} - \mu_{\text{non\_ex}})(\mu_{\text{ex}} - \mu_{\text{non\_ex}})^{\text{T}} \tag{5}$$

and S_{w} is the within-class scatter matrix:

$$S_{\text{w}} = S_{\text{ex}} + S_{\text{non\_ex}} \tag{6}$$

with μ_{ex} and $\mu_{\text{non\_ex}}$ the means of the exudate and non-exudate classes, respectively, estimated using the corresponding training set

$$\mu_{\text{ex}} = \frac{1}{N}\sum_{i=1}^{N} \boldsymbol{X}_{\text{ex}}^i \tag{7}$$

$$\mu_{\text{non\_ex}} = \frac{1}{M}\sum_{i=1}^{M} \boldsymbol{X}_{\text{non\_ex}}^i \tag{8}$$

and S_{ex} and $S_{\text{non\_ex}}$ the scatter matrices of each class:

$$S_{\text{ex}} = \sum_{i=i}^{N} (\boldsymbol{X}_{\text{ex}}^i - \mu_{\text{ex}})(\boldsymbol{X}_{\text{ex}}^i - \mu_{\text{ex}})^{\text{T}} \tag{9}$$

$$S_{\text{non\_ex}} = \sum_{i=i}^{M} (\boldsymbol{X}_{\text{non\_ex}}^i - \mu_{\text{non\_ex}})(\boldsymbol{X}_{\text{non\_ex}}^i - \mu_{\text{non\_ex}})^{\text{T}} \tag{10}$$

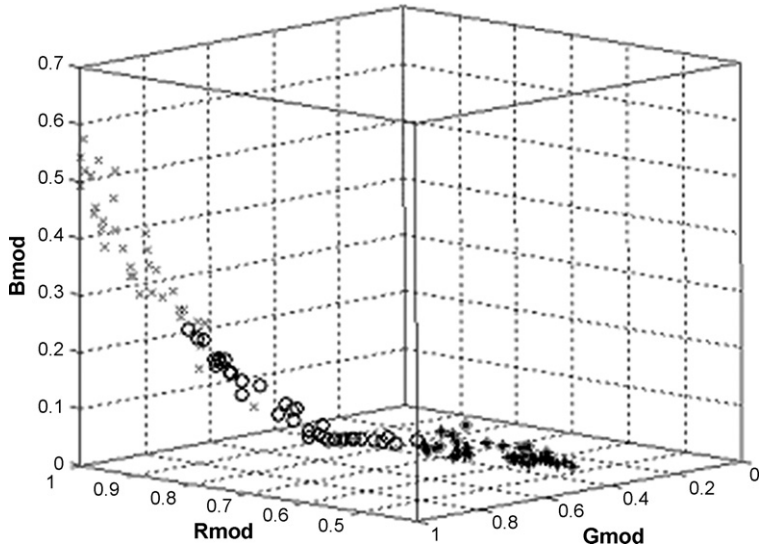

Fig. 2. Scatter plot of exudate pixel (x), pixels of the background around the OD (o) and pixel of the background far away from the OD (*).

The result after the classification task, I_{class}, is shown in Fig. 1(f).

2.4. Postprocessing stages

After the classification step, other yellow lesions such as cotton wool spots, OD, and artefacts near the papillary region are often present and may be erroneously detected as HEs. To avoid this problem, our algorithm contains a postprocessing stage specifically designed to provide robustness against the types of lesions and artefacts typically encountered in real clinical environments.

A significant attribute of HEs, in addition to their high intensity, is the sharpness of their edges. This characteristic is not representative of other elements such as cotton wool spots or artefacts in the papillary regions. Consequently, the algorithm makes use of the edge strength of the HEs to remove the yellow regions with blurred edges, such as cotton wool spots, detected in the classification stage during postprocessing. First, edges in the image are enhanced applying the Kirsch's method [18] to the original green component,

$$I_{\text{kirsch}}(m, n) = \max_k \{(\boldsymbol{g}_{mn} \cdot \boldsymbol{k}_k)\} \tag{11}$$

where $\boldsymbol{g}_{mn}$ is a vector which represents a 3×3 subimage of original green component centred in the pixel (m, n) and $\boldsymbol{k}_k$ with $k = 1, \ldots, 8$ are the group of masks which form the Kirsch operator. Using the Kirsch operator, the algorithm delineates the boundaries giving them a value that depends on the edge strength [18]. Thresholding the result at grey level α_1, only the sharpest edges are obtained, as it is shown in Fig. 1(g).

$$I_{\text{edge\_strength}} = T_{\alpha_1}(I_{\text{kirsch}}) \tag{12}$$

α_1 is an algorithm parameter that controls the trade-off between sensitivity and the number of false positives. Finally, $I_{\text{edge\_strength}}$ and I_{class}, the classification result, are combined with reconstruction by dilation operation to remove the yellow false positives [23].

The algorithm performs an automatic OD detection in order to mask out the OD region from the final result. The OD detection algorithm relies on two assumptions: (1) OD represents a bright region and (2) the primary four vessels normally emanate near-vertically from it. The method is composed of two parts:

1. Candidate selection using mathematical morphology,
2. OD detection using Hough transform.

A group of OD candidates are found applying alternative sequential filters to the modified luminance component Y_{mod}

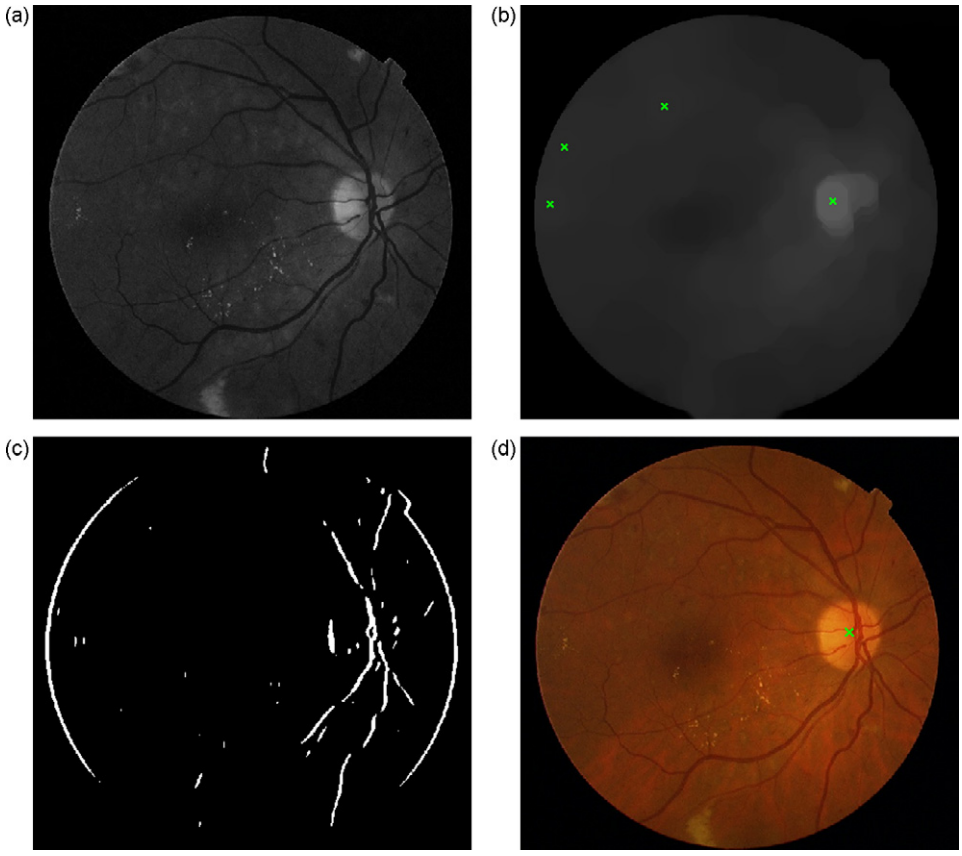

Fig. 3. Optic disk detection: (a) modified luminance component (Y_{mod}), (b) alternative sequential filtered image and regional maxima (in green), (c) vertical edges detected and (d) OD localization. (For interpretation of the references to color in this figure legend, the reader is referred to the web version of the article.)

to calculate the background approximation (Fig. 3(a–b)):

$$M = \mathrm{ASF}(Y_{\mathrm{mod}}) = \phi^{(nE)}(\ldots(\gamma^{(2E)}(\phi^{E}(\gamma^{E}(Y_{\mathrm{mod}}))))\ldots) \quad (13)$$

where ϕ and γ refer to grey closing and opening, respectively, and nE is an structuring element of size n sufficiently large to remove bright elements but not the OD [23]. The centroids of the regional maxima of M, shown in Fig. 3(b), represent the centres of potential ODs. In the second stage, a candidate is considered to be the OD if vertical vessels are found in its neighbourhood. First, vertical vessels are detected by matching Y_{mod} with a two-dimensional vertical-oriented filter characterized by a gaussian cross-profile section [24], as it is shown in Fig. 3(c). Each detected vessel is modelled by a single line to obtain the image skeleton. Then, the Hough transform is applied to the neighbourhood of the candidate centroids. The OD is the candidate region with the maximum number of pixels which belongs to vertical lines passing through it (Fig. 3(d)).

Fig. 1(h) depicts the final result of the algorithm after masking out the OD region.

3. System performance evaluation

Currently, there are no publicly available databases that can be used to assess the performance of automatic HE detection algorithms on retinal images. In this work, we assessed the performance of our algorithm using retinal images acquired from the *Instituto de Oftalmobiología Aplicada* at University of Valladolid, Spain. The images were obtained using a TopCon TRC-NW6S Non-Mydriatic Retinal Camera. Algorithm development and initial testing was performed using 25 retinal images. The algorithm was then validated prospectively using a database containing 58 unseen images (22 healthy retinas and 36 fundus images of diabetic subjects with HEs). In order to test the robustness of the algorithm in a clinical environment some of these images also included other signs of DR, such as haemorrhages and cotton wool spots. All the images were manually annotated by experts that identified HEs regions.

The algorithm performance was assessed using *Free-response receiver operating characteristic* (FROC) curves [25]. These curves show the true positive (TP) rate as a function of the number of false positive (FP) detections per image. A true exudate was considered found if the automatically detected cluster overlapped at least 50% of the area manually annotated by the expert. All findings outside this criterion were considered to be false detections.

4. Results

The algorithm was assessed using a lesion-based criterion. Fig. 4 shows the algorithm performance as a function of the segmentation threshold using the following simulation set:

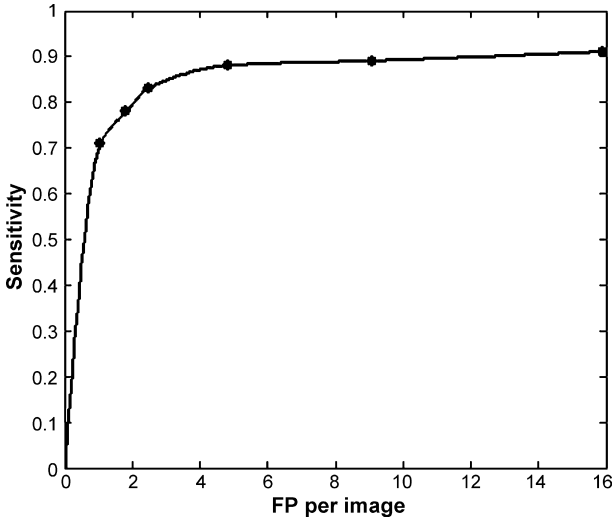

Fig. 4. FROC curve of lesion-based classification accuracy.

Table 2
Results of the exudate detection

α_1	Sensitivity	FP per image
0.5	0.91	15.92 ± 13.05
0.6	0.89	9.08 ± 7.96
0.7	0.88	4.83 ± 4.64
0.8	0.83	2.47 ± 2.70
0.9	0.78	1.83 ± 2.11
1	0.71	1.05 ± 1.49

$$\alpha_1 \in \{0.5,\ 0.6,\ 0.7,\ 0.8,\ 0.9,\ 1\} \quad (14)$$

These results indicate the algorithm achieves the best performances using a segmentation threshold of 0.7 ($\alpha_1 = 0.7$). Using this segmentation threshold the algorithm achieved a mean sensitivity of 88% with mean number of 4.83 ± 4.64 (mean ± standard deviation) false detections per image. Table 2 shows the algorithm sensitivity and specificity for other segmentation thresholds.

In addition to the lesion-based assessment, the proposed algorithm was also evaluated to determine its ability to distinguish (i.e. classify) between images containing HEs and healthy retinas (i.e. image-based criterion). The algorithm was able to successfully detect all the 36 images containing exudates using $\alpha_1 = 0.7$. Additionally, the proposed algorithm did not detect exudates in any of the 22 healthy retinas. This result indicates a sensitivity and a specificity of 100% based on image-based classification accuracy.

5. Discussion

5.1. Design considerations

One of the main challenges in the automatic identification of HEs is the wide variability of fundus colour among

different subjects. Past works partially avoided this problem by using only one of the image colour bands [9–12,16]. However, colour information is an important feature that can be used to distinguish among different lesions. Our proposed algorithm makes use of the colour information during the preprocessing stage and to achieve better performance in the image segmentation stage.

Retinal image characteristics contain important information to characterize the features of retinal lesions such as HEs. Consequently, preprocessing techniques are necessary to enhance the relevant features of retinal images. Simple approaches such as histogram equalization often fail due to wide variability in color, illumination, and contrast. A major drawback of histogram-based approaches such as histogram equalization and/or histogram specification as tools to perform retinal image enhancement is their sensitivity to colour. In these cases contrast or illumination are improved at the expense of fundus colour modification. Additionally, histogram-reshaping techniques such as histogram specification often mask evidence of lesions, since these are reflected in the original shape of the histogram [3]. Our proposed algorithm uses colour normalization together with contrast enhancement to achieve overall image enhancement without changing the chromatic properties of the input images. This enhancement is independent of external models and results in improvements adapted to the intrinsic characteristics of the retinal images. Additionally, the class separability of exudate and non-exudate pixels in this new colour space is increased compared with other colour models.

Selecting the appropriate training set is also important since it directly affects the performance of the algorithm. The approach we propose entails using different training sets automatically extracted for each image in order to take into account the large inter-image variability.

We evaluated the algorithm prospectively using an independent database of retinal images containing variable characteristics in order to investigate its robustness and its suitability for usage in a clinical environment. Retinal images of diabetic patients typically contain different clinical signs such as exudates, haemorrhages, microaneurysms and/or cotton wool spots. By choosing to evaluate the performance of the algorithm using images containing all these features we also evaluated the robustness of the algorithm in the presence of other lesions. The proposed algorithm is effective removing other yellow lesions, such as cotton wool spots. In 10 of the 36 fundus images of diabetic subjects with HEs, a total of 23 cotton wool spots (CWs) were present of which 15 of them were removed during the postprocessing step. Thus, the success rate of the CWs removal processing in the optimum operation point ($\alpha_1 = 0.7$) was 65%. The other 8 CWs could not be eliminated because they appear well contrasted in the images. However, this rate can be increased to 83% at the expense of decreasing the sensitivity (78%). Other yellow artefacts were also removed in this step, with a global success rate in the removal processing of 97%.

In this work, we used two different criteria to evaluate the algorithm performance: the lesion-based criterion and the image-based criterion. Using the lesion-based criterion, the accuracy is evaluated based on the number of exudate lesion detected in the image [17]. On the contrary, in image-based criteria, each image is examined looking for some evidence of DR (i.e. detecting the absence or presence of exudates anywhere in the image) [17]. Algorithms validated exclusively based on the image-based criterion typically report better performance since it is not necessary to detect all the exudates in the images to achieve a perfect classification. The British Diabetic Association recommends a minimum standard of 80% sensitivity and 95% specificity of detection of retinopathy signs by any method [26]. Other screening methods such as optometrists, Polaroids from non-mydriatic cameras, and diabetic physicians have reported sensitivity values varying from 61% to 97% and specificities from 78% to 96% [16]. Although our results are above these recommendations, the detection of exudates alone will not provide the necessary sensitivity for an acceptable eye-screening programme.

5.2. Validation databases

Due to the lack of a common database and a reliable way to measure performance, it is difficult to compare our algorithm to those previously reported in the literature. Although some authors [11,17] report algorithms with slightly better performance than our algorithm, these results may not be comparable, since these algorithms were assessed using different databases. Validation databases with manually annotated HEs by human experts are needed in order to provide reproducible and comparable performance assessment of HEs automatic image detection algorithms.

Our validation dataset will be publicly available at http://www.gib.tel.uva.es to provide other researchers a database to validate and compare their algorithms.

5.3. Algorithm limitations

The proposed algorithm makes uses of the isolated exudates colour to characterize yellowish regions. A limitation of this approach is that it cannot represent the colour of all the exudates found in images. A possible solution for this problem may be to detect exudates in different regions of the image and then use their colour to localize the rest of them. Additionally, despite the enhanced appearance of the HEs brought about by the preprocessing techniques, their diversity of brightness and size makes it difficult for an automatic algorithm to detect all of them. HEs usually appear in groups and therefore missing some of the very faint exudates is not critical. However, when there are only few very faint HEs in the retina, our proposed algorithm may have limited performance.

Finally, the database used to train the classifier and to evaluate the algorithm performance is not large enough to make general conclusions regarding the diagnostic value of

the algorithm. The algorithm should be assessed with more images in order to make the results more representative of the performance expected in a clinical setting.

6. Conclusion

We developed and prospectively validated an automatic image algorithm for HEs detection. The algorithm detects HE lesions based on colour, using a statistical classification; and by the sharpness of its edges, applying a Kirsch operator. Our results demonstrate that the system is well suited to complement the screening of DR and may be use to help the ophthalmologists in their daily practice.

Conflict of interest statement

There are no conflicts of interest that could inappropriately influence this research work.

References

[1] Singer DE, Nathan DM, Fogel HA, Schachat AP. Screening for diabetic retinopathy. Ann Intern Med 1992;116(8):660–71.
[2] Cree MJ, Olson JA, McHardy KC, Sharp PF, Forrester JV. The preprocessing of retinal images for the detection of fluorescein leakage. Phys Med Biol 1999;44(1):293–308.
[3] Cree MJ, Gamble E, Cornforth D. Colour normalisation to reduce inter-patient and intra-patient variability in microaneurysm detection in colour retinal images. In: Proceedings of the APRS Workshop on Digital Image Computing, vol. 163. 2005. p. 8.
[4] Foracchia M, Grisan M, Ruggeri A. Luminosity and contrast normalization in retinal images. Med Image Anal 2003;9(3):179–90.
[5] Pinz A, Prantl M, Datlinger P. Mapping the human retina. IEEE Trans Med Imaging 1998;17(4):606–19.
[6] Patton N, Aslam TM, MacGillivray T, Deary IJ, Dhillon B, Eikelboom RH, et al. Retinal image analysis: concepts, applications and potential. Prog Retin Eye Res 2006;25(1):99–127.
[7] Akita K, Kuga H. A computer method of understanding ocular fundus images. Pattern Recognition 1982;15(6):431–43.
[8] Kochner B, Schulman D, Obermaier M, Zahlmann G, Mann G, Englmeier KH. A image processing system for analyzing color fundus photographs with regard to diabetic retinopathy. Klinische Monatsblatter für Augenheilkunde 1997;211:11.
[9] Li H, Chutatape O. Automated feature extraction in color retinal images by a model based approach. IEEE Trans Biomed Eng 2004;51(2):246–54.
[10] Philips R, Forrester J, Sharp P. Automated detection and quantification of retinal exudates. Graefe's Archive for Clinical and Experimental Ophthalmology 1993;231(2):90–4.
[11] Walter T, Klein JC, Massin P, Erginay A. A contribution of image processing to the diagnosis of diabetic retinopathy—detection of exudates in color fundus images of the human retina. IEEE Trans Med Imaging 2002;21(10):1236–43.
[12] Ward NP, Tomlinson S, Taylor CJ. Image analysis of fundus photographs—the detection and measurement of exudates associated with diabetic retinopathy. Ophthalmology 1989;96:80–6.
[13] Zahlmann G, Kochner B, Ugi I, Schulhmann D, Liesenfeld B, Wegner A, et al. Hybrid fuzzy image processing for situation assessment: a knowledge-based system for early detection of diabetic retinopathy. IEEE Eng Med Biol Mag 2000;19(1):76–83.
[14] Goh KG, Hsu W, Lee ML, Wang H. ADRIS: an automatic diabetic retinal image screening system. In: Cios KJ, editor. Medical data mining and knowledge discovery. New York: Springer-Verlag; 2000. p. 181–210.
[15] Wang H, Hsu H, Goh G, Lee ML. An effective approach to detect lesions in color retinal images. In: Proceedings of the IEEE Conference on Computer Vision and Pattern Recogniton. 2000. p. 181–6.
[16] Gardner G, Leverton C, Young S, Lusty J, Dunstan F, Owens D. Automatic detection of diabetic retinopathy using an artificial neural network: a screening tool. Br J Ophthalmol 1996;80(11):940–4.
[17] Osareh A. Automated identification of diabetic retinal exudates and the optic disc. Ph.D. thesis. Bristol; 2004.
[18] Jain A. Fundamentals of digital image processing. New York: Prentice Hall; 1989.
[19] Goutsias J, Heijmans H, Sivakumar K. Morphological operators for image sequences. Computer Vision and Image Understanding 1995;62:326–46.
[20] Fukunaga K. Statistical pattern recognition. New York: Academic Press; 1990.
[21] Frei W, Chen CC. Fast boundary detection: a generalization and a new algorithm. IEEE Transactions on Computers 1977;26(10):988–98.
[22] Bishop CM. Neural network for pattern recognition. Oxford: Clarendon Press; 1997.
[23] Soille P. Morphological image analysis: principles and applications. New York: Springer-Verlag; 1999.
[24] Chaudhuri S, Chatterjee S, Katz N, Nelson M, Goldbaum M. Detection of blood vessels in retinal images using two-dimensional matched filters. IEEE Trans Med Imaging 1989;8(3):263–9.
[25] Chakraborty DP. The FROC, AFROC and DROC variants of the ROC analysis. In: Beutel J, Kundel HL, Van Metter RL, editors. Handbook of medical imaging, vol. 1. Bellingham: SPIE; 2000. p. 771–98.
[26] British Academic Association. Retinal photography screening for diabetic eye disease. London: British Academic Association; 1997.